Phantomless bone mineral density assessment in patients using dual-energy CT

Ryanne Offenberg

***Abstract*—**

OBJECTIVES – **To evaluate the accuracy of bone mineral density (BMD) measurement using various three-material decomposition approaches.**

METHODS – **Six three-material decomposition methods were developed to quantify BMD in the first lumbar vertebra of 15 patients. Virtual monoenergetic images at 50 and 200 keV were employed for the analyses. Spectral data were decomposed into calcium hydroxyapatite (HA), red bone marrow or water, and marrow adipose tissue. HA-based BMD measurements were compared to corresponding quantitative CT (QCT) results.**

RESULTS – **Strong linear correlations, but lack of agreement was found between the results obtained with the three-material decomposition methods and QCT. Spectral-based BMD values were substantially overestimated compared to QCT measurements. Average Hounsfield unit values at 50 and 200 keV inside the regions of interest suggested the presence of tissue that was not evaluated in the decomposition analyses. Furthermore, the three-material decomposition methods detected physiologically questionable volume fractions in some patients.**

CONCLUSIONS – **The three-material decomposition methods developed in this study show promising correlations with QCT, but further research is required to improve accuracy.**

***Index Terms*— Bone mineral density, Dual-energy CT, Dual-layer detector CT, Material decomposition, Osteoporosis.**

I. INTRODUCTION

Osteoporosis impairs the structural integrity of bone, increasing risks of fractures. Fractures can impact a patient's daily life substantially, in some cases fractures even have lethal consequences. Osteoporosis-related fractures can be prevented through treatment, but osteoporosis is often detected after a fracture has already occurred [1]. Opportunistic screening for bone mass degradation could detect osteoporosis in patients without symptoms, reducing underdiagnosis and preventing osteoporosis-related fractures with appropriate care.

Bone mass can be estimated by measuring the bone mineral density (BMD). The current gold standard for BMD assessment is dual-energy X-ray absorptiometry (DXA), a dedicated X-ray scan with low radiation exposure and cost [2], [3]. The method does come with several limitations. For instance, BMD is determined on a 2D projection image, which makes the measurement sensitive to overlying structures and degenerative changes in bones that artificially increase the BMD values [2], [3]. DXA measurements are also dependent on body size as it determines the areal BMD. Therefore, BMD measurements can be underestimated in small patients and overestimated in tall patients [2], [3]. Moreover, DXA is unable to differentiate between the compact cortical bone and porous trabecular bone [2]. Trabecular bone is more metabolically active, making this bone compartment more prone to BMD changes [3], [4].

Quantitative CT (QCT) is the current clinical standard for volumetric BMD measurements. Volumetric BMD values are independent of patient size [2]–[4]. Another advantage of QCT over DXA, is the ability to perform separate analyses of cortical and trabecular bone [2], [4]. However, QCT requires higher radiation exposure than DXA scans [2]. Additionally, several studies have indicated that QCT measurements are influenced by the amount of adipose tissue in bone marrow, resulting in BMD underestimation [4]–[6]. Moreover, QCT is dependent on the placement of a bone density calibration (BDC) phantom in the scanner, which can be easily forgotten. More importantly, placing a BDC phantom in the scanner is often only considered when there is suspicion of osteoporosis and most patients do not show symptoms of decreased BMD, even though they may be at risk of fractures.

Bone density assessment using dual-energy CT (DECT) has been studied in recent years [7]–[11]. More information can be captured using DECT as attenuation values are obtained at two different energies. Materials with different attenuation properties at certain energies can thus be distinguished and quantified. This could enable the ability to quantify BMD without the need for a phantom, while also accounting for marrow fat. Like QCT, DECT performs a volumetric BMD measurement and allows separate analyses of cortical and trabecular bone.

Most DECT acquisition methods, such as single-source rapid kilovoltage switching and dual-source CT, are prospective techniques that require a specific acquisition protocol. A dual-layer detector CT (DLCT) system has been developed more recently. Dual-layer energy information is always acquired with a DLCT system, no specific acquisition protocol is required. Additionally, it does not expose the patient to a higher radiation dose compared to a conventional single-layer detector CT [12]. DLCT could enable opportunistic screening of bone mass, eliminating the need for an additional DXA or CT scan [7], [13].

A previous study has indicated the potential of a three-material decomposition method to assess BMD in DECT images without the influence of soft tissue and fat [14]. Material decomposition is a way to quantify specific materials in an image using their distinctive attenuation properties at different energies. A three-material decomposition method has also been

This work was submitted for review on the 1st of October 2021.
Ryanne Offenberg is with the Image Sciences Institute, University Medical Center Utrecht, Utrecht University, 3508 GA Utrecht, The Netherlands (e-mail: r.offenberg@students.uu.nl).

successfully implemented to differentiate acute and chronic thoracolumbar vertebral fractures based on the level of bone marrow oedema [8]. Therefore, a three-material decomposition method possibly enables phantomless quantification of BMD while eliminating the confounding effect of fatty tissue.

The aim of this pilot study was to evaluate the performance of various three-material decomposition approaches to quantify BMD in patients.

II. Materials and Methods

A. Study population and phantoms

A selection of 15 patients was included in this pilot study. All patients suffered from pseudoxanthoma elasticum (PXE), a rare genetic disorder that affects the skin, eyes, and blood vessels [15]. As far as we currently know, PXE does not impact the BMD. Patients were included if images were acquired with a DLCT system, scans were not contrast-enhanced, spectral-based imaging (SBI) data was available, and a BDC phantom was present in the scan. Patient characteristics can be found in Table I. All patients underwent a full body CT examination with the presence of a BDC phantom (QRM GmbH, Moehrendorf, Germany) in a DLCT scanner between January 2020 and April 2021.

Every patient was scanned with a BDC phantom under their knee (Fig. 1). This allowed to perform a QCT analysis by converting Hounsfield Units (HU) into BMD values through a linear regression analysis on the BDC phantom. The phantom contained three cylindrical inserts with different concentrations of calcium hydroxyapatite (HA), approximately 0, 100 and 200 mg/cm^3 HA. The specific phantom used in this study consisted of 0, 98.5 and 198.6 mg/cm^3 HA. Base materials for the phantom inserts consisted of a water-equivalent plastic, which has the same attenuation properties as water. The material surrounding the inserts was a soft-tissue-equivalent plastic.

B. DLCT imaging protocols

Total-body images were obtained with a dual-layer spectral detector CT scanner (iQon Spectral CT, Philips Healthcare, Best, The Netherlands). The top layer of the dual-layer detector absorbs low-energy photons, while the bottom layer collects data from high-energy photons. SBI can thus be reconstructed. Based on SBI, conventional and virtual monoenergetic (monoE) images can be retrospectively generated.

A spiral acquisition mode was used with a tube peak voltage of 120 kVp, 0.984 pitch factor, gantry revolution time of 0.75 s and 64x0.625 collimation. Dose modulation was employed to limit radiation exposure by adapting the tube current to the patient's size while maintaining the same signal-to-noise ratio.

Table I.
Sex and age (mean ± standard deviation (SD)) of included patients

	Number of patients	Age
All	15	55 ± 13 years
Male	10	53 ± 14 years
Female	5	60 ± 12 years

Average exposure among patients was 23.5 ± 9.2 mAs (mean ± SD) and mean CT dose indices ($CTDI_{vol}$) were 2.1 ± 0.8 mGy. Conventional and monoE images at 50 and 200 keV were reconstructed using the SBI with a standard filter kernel (B) and slice thickness of 1 mm [10].

Regions of interest (ROIs) were placed on the ventral side of the trabecular bone compartment just inferior to the superior endplate of the first lumbar vertebra. All ROI placements were verified by a radiologist. An example of the ROI location can be seen in Fig. 2. The ROIs consisted of 2D circles that were placed on three consecutive slices in axial view. ROIs were 14.3 mm in diameter and consisted of 507 voxels, corresponding to a volume of 421.8 to 483.5 mm^3 depending on the voxel dimensions of the images. The BMD within the ROI was determined with QCT, as well as a three-material decomposition method.

C. BMD quantification based on a three-material decomposition

A three-material decomposition was used to assess the BMD in spectral data, without the need of a phantom. In this method, the volume fractions of each material were assessed in every voxel. The average volume fraction of HA within the ROI was used to determine the BMD by multiplying the volume fraction with the density of HA. The software used for the three-material decomposition analyses was in-house developed.

Two combinations of materials were evaluated in the analyses to established the difference in performance. Pure HA and marrow adipose tissue (MAT) were used in combination with either red bone marrow (RBM) or water. These materials were selected as attenuation values for HA, RBM, and MAT were successfully used in the three-material decomposition method presented by Hofmann *et al*., and attenuation properties of HA and water were used in the two-material decomposition by Van Hamersvelt *et al*. [7], [14]. The attenuation coefficient for each material at 50 and 200 keV were obtained from the International Commission on Radiation Units and Measurement Report 46 [16].

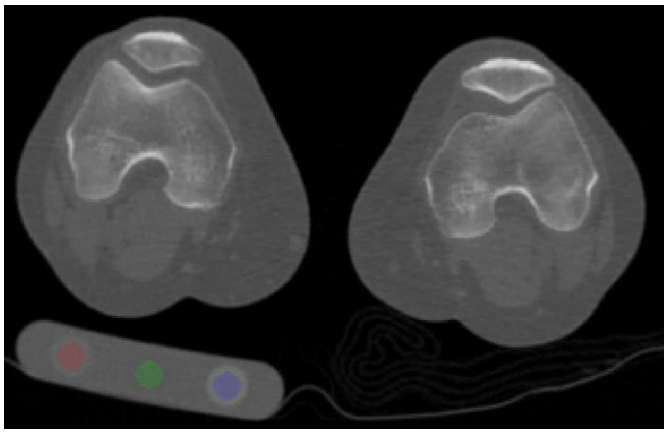

Fig. 1. BDC phantom placed under the knee of a patient, visualized in a conventional DLCT image. ROIs are placed within the three inserts for the QCT method.

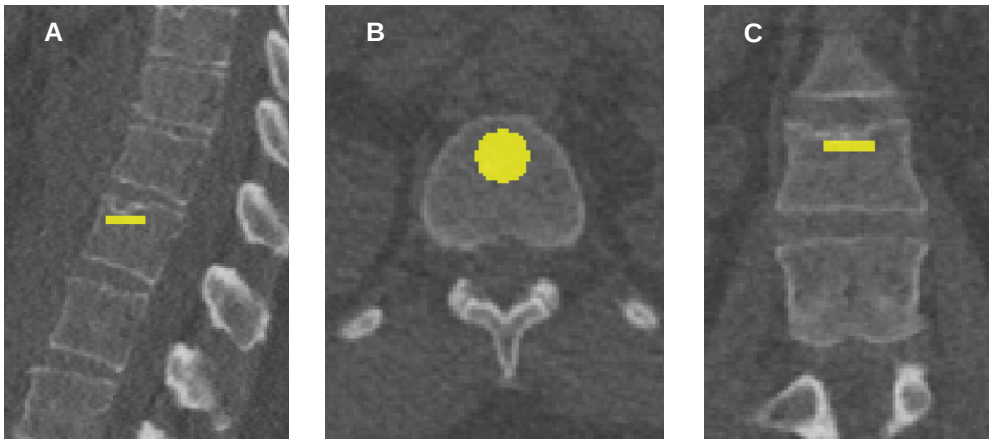

Fig. 2. ROI placement depicted in (**A**) sagittal, (**B**) axial, and (**C**) coronal plane of a conventional DLCT image from a patient.

For both monoE images, HU values were converted into attenuation coefficients using the following formula:

$$\mu(E) = \frac{HU(E) * \mu_{water}(E)}{1000} + \mu_{water}(E) \quad (1)$$

Where E is the energy of the monoE image, μ(E) is the attenuation coefficient at energy E, HU(E) is the HU value in the monoE image, and μ_{water} is the attenuation coefficient of water at energy E.

Volume fractions were determined based on the attenuation coefficients in the two monoE images, as well as the assumption of volume conservation. The sum of volume fractions is assumed to equal the volume of the combined materials at the same pressure and temperature. This assumption introduced a third linear equation that enabled the ability to find a solution for the three unknown volume fractions.

$$\mu(E_1) = \mu_{m1}(E_1) * f_1 + \mu_{m2}(E_1) * f_2 + \mu_{m3}(E_1) * f_3 \quad (2)$$

$$\mu(E_2) = \mu_{m1}(E_2) * f_1 + \mu_{m2}(E_2) * f_2 + \mu_{m3}(E_2) * f_3 \quad (3)$$

$$f_1 + f_2 + f_3 \approx 1 \quad (4)$$

E_1 is 50 keV and E_2 is 200 keV, $\mu(E_x)$ is the attenuation coefficient in the monoE image, $\mu_{mx}(E_x)$ the known attenuation coefficient for the specific material at the particular energy, and f_x is the volume fraction corresponding to the material.

This system of linear equations was solved using two different approaches. In one of the approaches, a non-negative least square (NNLS) function was implemented [17], [18]. The aim of this NNLS method was to identify the smallest possible volume fractions that are greater or equal to zero. The other method aimed to minimize the norm of Ax-b, where A is are the known attenuation coefficients for the materials, x are the volume fractions and b are the attenuation coefficient found in the monoE images [18]. Volume fractions were bound by [0,1]. The minimize method was either constrained by a sum of volume fractions that equals one (sum=1), or by a sum of fractions that was larger or equal to 0.95 (sum≥0.95). This last constraint was chosen because the attenuation in the image can be affected by noise, therefore it does not always make sense that the sum of material attenuations corresponds exactly to the attenuation in the image. Thus, six three-material decomposition methods were evaluated in total.

D. BMD gold standard quantification using QCT

A BDC phantom was used to convert HU values in the conventional image to BMD values. The phantom contained three inserts with known HA concentrations, in which cylindrical ROIs were placed along the length of the phantom (Fig. 1). Average values within these ROIs were used to construct a calibration curve with which the conventional image could be converted into a BMD map. BMD gold standard values could thus be extracted from the ROI in the BMD image. The software employed for this analysis was in-house developed.

E. Statistical analysis

Shapiro-Wilk tests were performed to confirm a normal distribution of data. Linear correlations between the three-material decompositions and QCT results were assessed by calculating the Pearson correlation coefficient. Linear regression analyses were also performed to evaluate the relationship between QCT and three-material decomposition results. Bland-Altman plots were generated to evaluate agreement and any possible trends between the three-material decomposition methods and QCT.

III. Results

Strong linear correlations were found between BMD values obtained with QCT and all three-material decomposition methods, see Table II and Fig. 3. BMD values determined by the NNLS method evaluating the combination of HA, RBM, and MAT, showed the lowest correlation with QCT results, followed by the norm minimizing (sum≥0.95) method that analysed the same materials. The other methods demonstrated Pearson correlation coefficients greater than 0.9 and coefficients of determination over 0.8. The linear regression analyses displayed in Fig. 3 visualize these strong correlations between QCT and the spectral-based results. The plots also show an overestimation in BMD values obtained with the three-material decomposition methods compared to QCT.

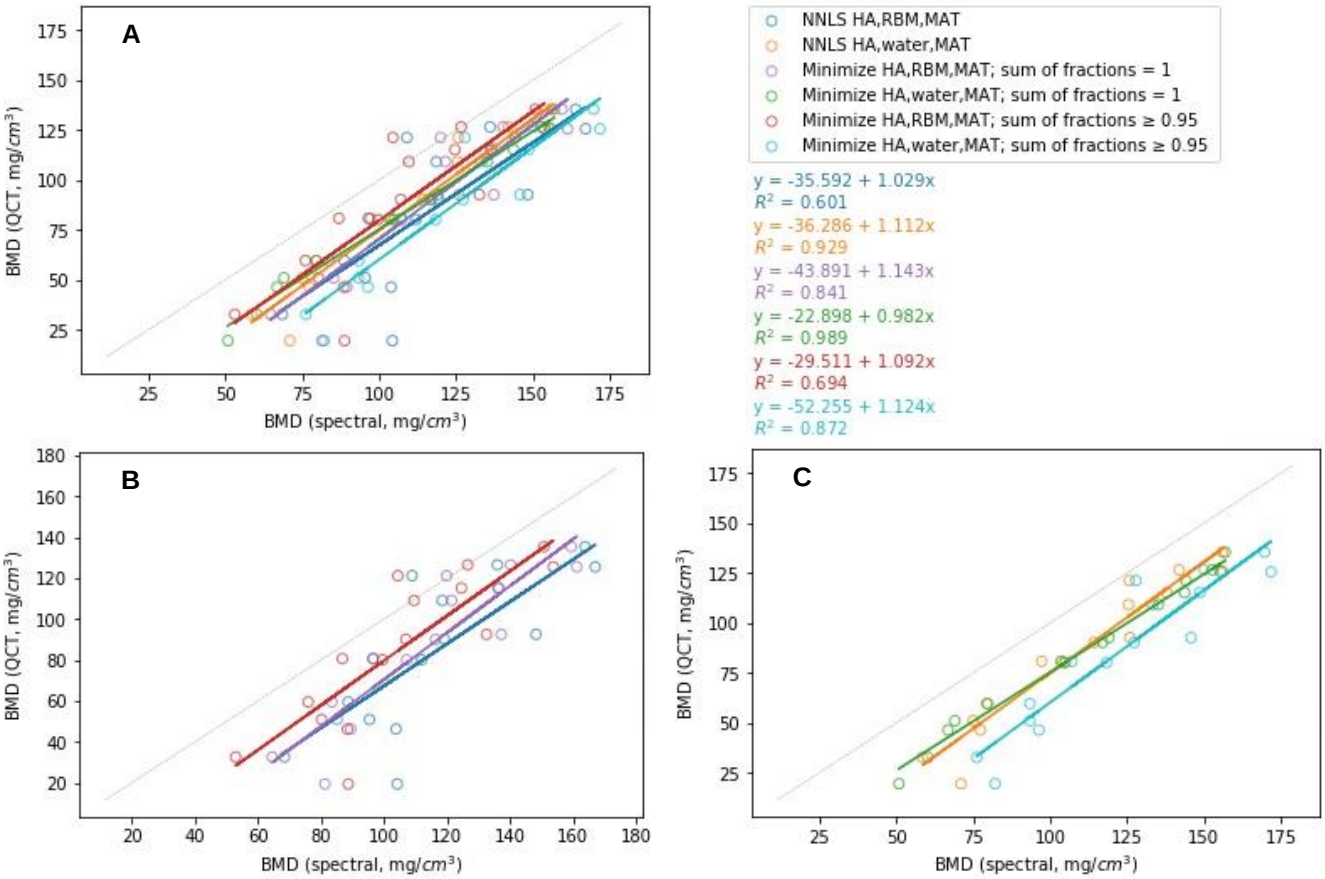

Fig. 3. BMD values quantified in patients using QCT and a three-material decomposition. (**A**) Full linear regression plot presenting all the analysed three-material decomposition methods. BMD values acquired with QCT and the three-material decomposition methods demonstrated a strong correlation. But there is also a clear overestimation in BMD values obtained with three-material decomposition methods compared to QCT. (**B, C**) For clarity, a selection of methods in which HA, RBM, and MAT were evaluated is presented in section B. A selection of methods in which HA, water, and MAT were examined is shown in section C.

Table II.
Linear correlations between BMD values assessed with QCT and the three-material decomposition methods.

Materials	Method	Pearson correlation coefficient
HA, RBM, MAT	NNLS	0.776
	Minimize (sum=1)	0.917
	Minimize (sum≥0.95)	0.834
HA, water, MAT	NNLS	0.964
	Minimize (sum=1)	0.995
	Minimize (sum≥0.95)	0.934

The Bland-Altman plots in Fig. 4 show a positive bias between the mean BMD difference obtained with QCT and three-material decomposition methods. Moreover, average BMD differences between QCT and most three-material decomposition methods increased at lower averages of the two BMD values. This negative trend was less clear in the minimize (sum=1) method in which HA, water, and MAT were examined. The variability in BMD difference was smallest for that same method, all mean values were within the 95% confidence interval. In other methods, either one or two average values fell outside of the limits of agreement (±1.96 SD). The smallest mean difference with QCT results was obtained with the minimize (sum≥0.95) method in which HA, RBM, and MAT were evaluated, while the largest bias was found in the same method in which the HA, water, and MAT were analysed.

To get more insight into why the three-material decomposition methods consistently obtained higher BMD values compared to QCT, the HU values of the evaluated materials and the average HU value in the ROIs of the patients at 50 and 200 keV were plotted (Fig. 5). The pure materials form a triangle. If the tissues within the ROI consisted purely of the three selected materials, average ROI values would fall inside the triangle. Because water, MAT, and RBM, have relatively similar attenuation values at both 50 and 200 keV, the two triangles of pure materials are similar. In 5 out of 15 patients, average ROI values were completely outside both triangles. The average value of 4 patients was located inside the HA, RBM, and MAT triangle, while only the average of 1 patient's ROI was located completely inside the HA, water, and MAT triangle.

In addition to the triangle plots, the relation between material volume fractions and BMD values obtained with QCT and the spectral-based methods was investigated (Fig. 6). For the NNLS and minimize (sum=1) method that assessed the volume

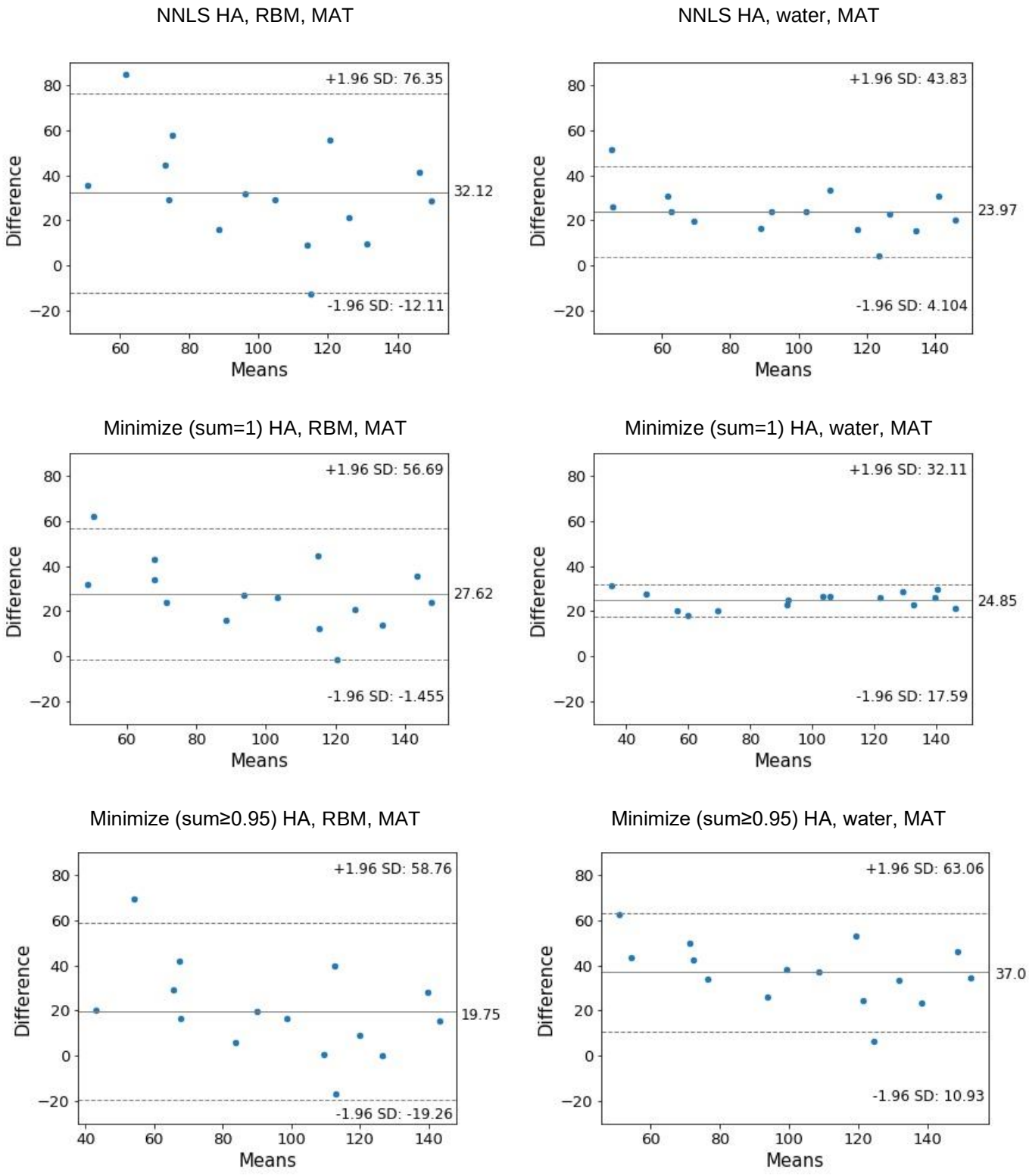

Fig. 4. Bland-Altman plots depicting the means and differences in BMD acquired with QCT and the three-material decomposition methods in patients. Values are in mg/cm^3 HA. The mean BMD difference (spectral-based method – QCT) is indicated with a solid line, limits of agreement (mean ± 1.96 SD) are represented by the dashed lines. All methods present a bias between +19.75 and +37.0. A negative trend is visible in all plots, except the plot depicting the agreement between QCT and the minimize (sum=1) method that evaluated HA, water, and MAT.

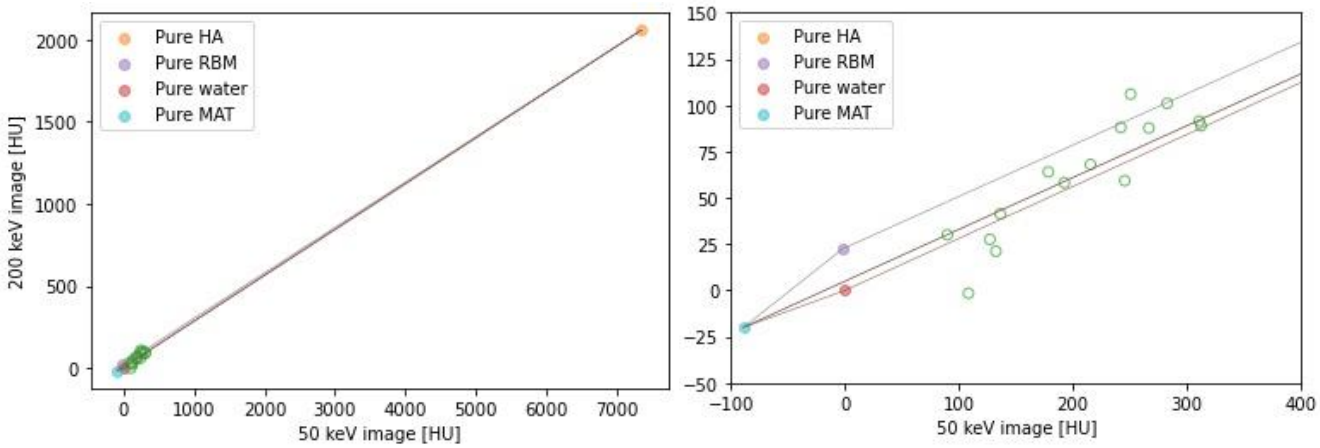

Fig. 5. Scatterplot displaying the HU values of the investigated materials in the 50 and 200 keV monoE images. The open green circles correspond to the average HU values in the ROI of patients. Left: full plot; right: zoomed in plot.

fractions for HA, RBM, and MAT, differences in BMD increased with increasing MAT content and decreasing RBM fractions. The opposite trend was seen in the NNLS method that evaluated HA, water, and MAT. No clear pattern was found in the minimize (sum=1) method that quantified volume fractions for HA, water, and MAT. But the difference in BMD values obtained with that method and QCT appeared more constant than in other three-material decomposition approaches. The plots for the minimize (sum≥0.95) method differed substantially from the other methods. RBM volume fractions were estimated to exceed 0.7 in most patients when examining HA, RBM, and MAT. Similar volume fractions were quantified for MAT when HA, water, and MAT were evaluated.

The same figures were analysed from the perspective in which patients were sorted based on their age and sex. Here, only a trend of declining BMD values with older age was found.

IV. Discussion

The performance of six different three-material decomposition methods to assess BMD in patients was evaluated and compared to QCT-based BMD measurements. Strong correlations but lack of agreement was found between QCT and three-material decomposition results. BMD measurements performed by three-material decomposition methods were generally higher than corresponding QCT results. The reason for this overestimation remains mostly unclear. Analyses indicate that the choice of evaluated materials may have been incorrect. Future research is required to improve the accuracy and stability of the three-material decomposition before this method can be employed for opportunistic screening.

When comparing the performance of the three-material decomposition methods to QCT, the norm minimization (sum=1) method that quantified volume fractions for HA, water, and MAT performed best. Results of this method had the highest correlation coefficient ($r > 0.99$) and coefficient of determination ($r^2 = 0.99$) with QCT results, as well as the least variability in difference with BMD values obtained with QCT. The NNLS method that assessed volume fractions of HA, RBM, and MAT performed the worst. It had the smallest correlation coefficient ($r = 0.78$) and coefficient of determination ($r^2 = 0.60$), the second biggest average difference results with QCT with the most variance among the evaluated methods. In general, the methods that investigated volume fractions for HA, water, and MAT outperformed the methods evaluating HA, RBM, and MAT.

Even though good linear correlations were found, BMD values assessed with three-material decompositions were considerably higher than their corresponding QCT-based results. The American College of Radiology presents cut off values based on world health organisation (WHO) DXA guidelines, since no WHO QCT-based diagnostic guidelines currently exist. Osteoporosis is indicated when BMD in the spine is below 80 mg/cm^3 HA, osteopenia for BMD between 80 and 120 mg/cm^3 HA, and BMD values over 120 mg/cm^3 HA are considered normal [19]. Average BMD differences between QCT and spectral-based methods of 20 and 37 mg/cm^3 HA are therefore substantial. The three-material decomposition employed by Hofmann *et al.* did not detect higher BMD values compared to QCT. Instead, the study mentions BMD measurements in some patients were substantially lower compared QCT but in agreement with parallel DXA, their gold standard [14].

To gain more insight into the reason of this bias, the HU values of the investigated materials and average ROI values in patients at 50 and 200 keV were plotted (Fig. 5). The values of pure materials create a triangle, all possible combinations of these pure materials exist inside the triangle. But only a few patients' mean values were located within such a triangle. This indicates that different tissues are present within the ROI, because of partial volume effect or due to the incorrect choice of materials. Generally, three-material decomposition methods obtained more comparable BMD values to QCT in patients whose mean ROI value were closer or inside the triangle. But this trend was most noticeable in methods that evaluated HA, RBM, and MAT, which would correspond to the wider triangle plot. Additionally, noise could affect the average ROI values.

The triangle plots also displayed the similarity between RBM, water, and MAT attenuation values at 50 and 200 keV. This is because both RBM and MAT are composed of fat, water, and protein. The chemical composition of MAT in adults is

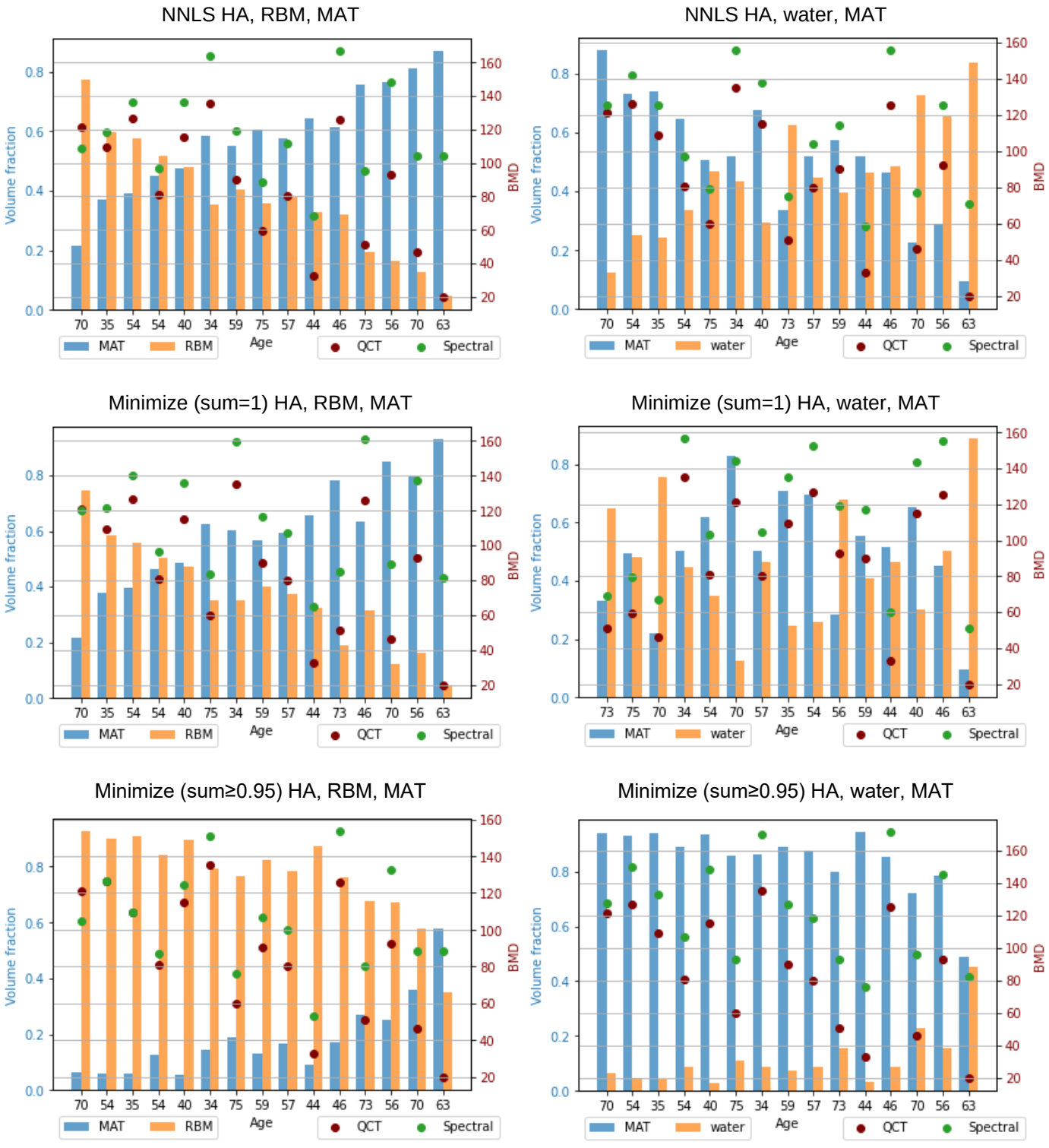

Fig. 6. BMD results obtained with QCT and a three-material decomposition in relation to the volume fractions of RBM or water, and MAT. Patients are presented on the x-axis, where the labels refer to the age of the patients. Volume fractions of MAT and either RBM or water are represented by the bar plots. The left side of the y-axis can be used to read the volume fractions. BMD values are represented by the open circles, which values can be read on the right side of the y-axis. Patients are sorted left to right from smallest to biggest difference between BMD values obtained with QCT and the three-material decomposition method.

80% fat, 15% water, and 5% proteins. Whereas RBM consists of 40% fat, 40% water, and 20% proteins in adults [20]. Previous studies have indicated that a small differences in HU values can result in substantial differences in the quantification of materials [5], [14]. Especially materials with similar attenuation properties, e.g. RBM, water, and MAT, will be sensitive to this effect. Future research should focus on improving this by quantifying volume fractions of physiologically relevant materials that have more distinctive attenuation properties. In addition, physiological constraints on the material concentrations could help and prevent biologically implausible volume fractions, which were detected in this study. The analysis involving the relation between BMD results and quantified volume fractions for RBM or water, and MAT, showed that the minimize (sum≥0.95) obtained unrealistic volume fractions for RBM and water. Other methods also detected questionable RBM-MAT and water-MAT ratios. Sfeir *et al.* implemented a physiological restriction in which fat concentration was limited by 0 and 600 mg/cm^3 [5]. It should be noted that physiological constraints would have to account for the dynamic composition of bone marrow among patients [20], [21].

When MAT volume fractions increased, according to the NNLS and minimize (sum=1) method that quantified volume fractions for HA, RBM, and MAT, BMD differences with QCT increased as well. BMD values obtained by QCT were generally smaller when the aforementioned spectral-based methods detected high MAT volume fractions. This makes sense as higher contents of MAT are found in osteoporotic patients [6], [22]. But QCT is also known to underestimate BMD values due to increased MAT content, which is accounted for in the three-material decomposition methods [5], [23]. To investigate the extend of the effect of MAT on BMD values, Sfeir *et al.* compared single-energy (SE) and dual-energy (DE) QCT performance in the trabecular bone compartment of the lumbar spine and both trabecular and cortical compartments of the femoral neck. The DE QCT method employed a three-material decomposition, evaluating volume fractions of HA, RBM, and MAT to account for marrow fat. DE QCT BMD values were higher than SE QCT values, especially in the trabecular bone compartments. The BMD difference in trabecular bone of the lumbar spine was 17.6%. This difference was substantially smaller in the cortical bone compartment, where MAT is lacking. The underestimation of SE QCT compared to DE QCT increased with lower BMD values, a similar trend was seen in the Bland-Altman plots in our study [5].

Other methods to determine BMD using DLCT scans have been proposed. Van Hamersvelt *et al.* performed a two-material decomposition, analysing HA and water, on spectral images acquired with a DLCT system to measure BMD in an anthropomorphic spine phantom. BMD values were compared to DXA results and showed high accuracy. A different approach was used by Mei *et al.* to determine BMD in similar anthropomorphic spine phantom and vertebral specimens. The same assumption was made that ROIs were composed of only HA and water. Using the relationship between 50 and 200 keV monoE images and a calibration equation based on one BDC phantom scan, HU values in the ROI were converted to BMD values. This method performed highly accurate in phantom data. In vertebral specimen, high correlations and agreement were found between QCT and spectral-based results. Roski *et al.* employed a similar method to determine BMD values in 33 patients, which showed comparable results to QCT. Although these methods show promising results, MAT was not explicitly accounted for in any of these methods.

This study has several limitations. A small number of patients were included in this study due to the limited time available to reconstruct virtual monoenergetic images. The selection was made with intention to retain a wide range of different BMD values, which was based on QCT results that were obtained on data of 42 patients that fit the inclusion requirements. Including more patient data would improve the reliability of the analyses and the potential to extrapolate the results to a wider patient population. Second, we did not have a reference standard that could be used to compare volume fractions of RBM, water, or MAT to. In future studies, magnetic resonance imaging could be employed to determine the content of bone marrow. A third limitation is that this study did not account for intravenous contrast media. In the prospect of opportunistic BMD screening, methods should be able to account for contrast-enhanced images [24].

In conclusion, different approaches to a three-material decomposition were presented in this study. Strong linear correlations, but lack of agreement was found between QCT and three-material decomposition methods All three-material decomposition methods showed an overestimation in BMD results compared to QCT. More research is required to improve the accuracy of the three-material decomposition.

V. Acknowledgement

I thank my supervisors, dr. ir. Koen Vincken and dr. Graeme Campbell (Philips Healthcare), for their ideas and guidance throughout the project. I also thank dr. Wouter Foppen and prof. dr. Pim de Jong for their medical insight, as well as dr. Arnold Schilham for sharing his expertise on the subject.

VI. References

[1] F. Cosman *et al.*, "Clinician's Guide to Prevention and Treatment of Osteoporosis," *Osteoporos. Int.*, vol. 25, no. 10, p. 2359, Sep. 2014, doi: 10.1007/S00198-014-2794-2.

[2] T. M. Link and G. Kazakia, "Update on Imaging-Based Measurement of Bone Mineral Density and Quality," *Current Rheumatology Reports*, vol. 22, no. 5. Springer, May 01, 2020, doi: 10.1007/s11926-020-00892-w.

[3] T. M. Link, "Radiology of Osteoporosis," *Canadian Association of Radiologists Journal*, vol. 67, no. 1. Canadian Medical Association, pp. 28–40, Feb. 01, 2016, doi: 10.1016/j.carj.2015.02.002.

[4] J. E. Adams, "Quantitative computed tomography," *Eur. J. Radiol.*, vol. 71, no. 3, pp. 415–424, Sep. 2009, doi: 10.1016/j.ejrad.2009.04.074.

[5] J. G. Sfeir *et al.*, "Evaluation of Cross-Sectional and Longitudinal Changes in Volumetric Bone Mineral Density in Postmenopausal Women Using Single- versus Dual-Energy Quantitative Computed Tomography," *Bone*, vol. 112, p. 145, Jul. 2018, doi: 10.1016/J.BONE.2018.04.023.

[6] Y. Sheu and J. A. Cauley, "The Role of Bone Marrow and Visceral Fat on Bone Metabolism," *Curr. Osteoporos. Rep.*, vol. 9, no. 2, p. 67, Jun. 2011, doi: 10.1007/S11914-011-0051-6.

[7] R. W. van Hamersvelt *et al.*, "Accuracy of bone mineral density quantification using dual-layer spectral detector CT: a phantom

study," *Eur. Radiol.*, vol. 27, no. 10, pp. 4351–4359, Oct. 2017, doi: 10.1007/s00330-017-4801-4.

[8] B. J. Schwaiger *et al.*, "Three-material decomposition with dual-layer spectral CT compared to MRI for the detection of bone marrow edema in patients with acute vertebral fractures," *Skeletal Radiol.*, vol. 47, no. 11, pp. 1533–1540, Nov. 2018, doi: 10.1007/s00256-018-2981-x.

[9] D. K. Mueller, A. Kutscherenko, H. Bartel, A. Vlassenbroek, P. Ourednicek, and J. Erckenbrecht, "Phantom-less QCT BMD system as screening tool for osteoporosis without additional radiation," *Eur. J. Radiol.*, vol. 79, no. 3, pp. 375–381, Sep. 2011, doi: 10.1016/j.ejrad.2010.02.008.

[10] F. Roski *et al.*, "Bone mineral density measurements derived from dual-layer spectral CT enable opportunistic screening for osteoporosis," *Eur. Radiol.*, vol. 29, no. 11, pp. 6355–6363, Nov. 2019, doi: 10.1007/s00330-019-06263-z.

[11] K. Mei *et al.*, "Bone mineral density measurements in vertebral specimens and phantoms using dual-layer spectral computed tomography," *Sci. Rep.*, vol. 7, no. 1, pp. 1–10, Dec. 2017, doi: 10.1038/s41598-017-17855-4.

[12] F. Van Ommen, H. W. A. M. De Jong, J. W. Dankbaar, E. Bennink, T. Leiner, and A. M. R. Schilham, "Dose of CT protocols acquired in clinical routine using a dual-layer detector CT scanner: A preliminary report," 2019, doi: 10.1016/j.ejrad.2019.01.011.

[13] S. Van Hedent *et al.*, "Improving Bone Mineral Density Assessment Using Spectral Detector CT," *J. Clin. Densitom.*, vol. 22, no. 3, pp. 374–381, Jul. 2019, doi: 10.1016/j.jocd.2018.10.004.

[14] P. Hofmann *et al.*, "Phantom-less bone mineral density (BMD) measurement using dual energy computed tomography-based 3-material decomposition," *Med. Imaging 2016 Comput. Diagnosis*, vol. 9785, p. 97853E, 2016, doi: 10.1117/12.2217413.

[15] D. P. Germain, "Pseudoxanthoma elasticum," *Orphanet J. Rare Dis. 2017 121*, vol. 12, no. 1, pp. 1–13, May 2017, doi: 10.1186/S13023-017-0639-8.

[16] D. R. White, R. V. Griffith, and I. J. Wilson, "Report 46," *J. Int. Comm. Radiat. Units Meas.*, vol. os24, no. 1, p. NP-NP, Feb. 1992, doi: 10.1093/JICRU/OS24.1.REPORT46.

[17] C. L. Lawson and R. J. Hanson, *Solving least squares problems*. SIAM, 1995.

[18] P. Virtanen *et al.*, "{SciPy} 1.0: Fundamental Algorithms for Scientific Computing in Python," *Nat. Methods*, vol. 17, pp. 261–272, 2020, doi: 10.1038/s41592-019-0686-2.

[19] The American College of Radiology, "Acr–Spr–Ssr Practice Parameter for the Performance of Musculoskeletal Quantitative Computed Tomography (Qct)," vol. 1076, no. (Resolution 9), p. 6, 2018.

[20] B. C. Vande Berg, J. Malghem, F. E. Lecouvet, and B. Maldague, "Magnetic resonance imaging of normal bone marrow," *Eur. Radiol.*, vol. 8, no. 8, pp. 1327–1334, 1998, doi: 10.1007/S003300050547.

[21] A. Małkiewicz and M. Dziedzic, "Bone marrow reconversion – imaging of physiological changes in bone marrow," *Polish J. Radiol.*, vol. 77, no. 4, p. 45, 2012, doi: 10.12659/PJR.883628.

[22] J. F. Griffith *et al.*, "Vertebral Marrow Fat Content and Diffusion and Perfusion Indexes in Women with Varying Bone Density: MR Evaluation1," *https://doi.org/10.1148/radiol.2413051858*, vol. 241, no. 3, pp. 831–838, Dec. 2006, doi: 10.1148/RADIOL.2413051858.

[23] X. Cheng *et al.*, "Correction of QCT vBMD using MRI measurements of marrow adipose tissue," 2019, doi: 10.1016/j.bone.2018.12.015.

[24] E. Pompe, M. J. Willemink, G. R. Dijkhuis, H. J. J. Verhaar, F. A. A. M. Hoesein, and P. A. de Jong, "Intravenous contrast injection significantly affects bone mineral density measured on CT," *Eur. Radiol.*, vol. 25, no. 2, pp. 283–289, Feb. 2015, doi: 10.1007/s00330-014-3408-2.